JOURNAL OF GEOPHYSICAL RESEARCH, VOL. 94, NO. A10, PAGES 13,397–13,408, OCTOBER 1, 1989

High-Frequency Electrostatic Waves Near Earth's Bow Shock

T. G. ONSAGER,[1,2] R. H. HOLZWORTH,[1] H. C. KOONS,[3] O. H. BAUER,[4]
D. A. GURNETT,[5] R. R. ANDERSON,[5] H. LÜHR,[6] AND C. W. CARLSON[7]

Electrostatic wave measurements from the Active Magnetospheric Particle Tracer Explorer Ion Release Module have been used to investigate the wave modes and their possible generation mechanisms in the Earth's bow shock and magnetosheath. It is demonstrated that electrostatic waves are present in the bow shock and magnetosheath with frequencies above the maximum frequency for Doppler-shifted ion acoustic waves, yet below the plasma frequency. Waves in this frequency range are tentatively identified as electron beam mode waves. Data from 45 bow shock crossings are then used to investigate possible correlations between the electrostatic wave properties and the near-shock plasma parameters. The most significant relationships found are anticorrelations with Alfven Mach number and electron beta. Mechanisms which might produce electron beams in the shock and magnetosheath are discussed in terms of the correlation study results. These mechanisms include acceleration by the cross-shock electric field and by lower hybrid frequency waves. A magnetosheath "time of flight" mechanism, in analogy to the electron foreshock region, is introduced as another possible beam generation mechanism.

1. INTRODUCTION

High-frequency electrostatic wave turbulence is a common feature of the Earth's bow shock. Since its discovery [*Fredricks et al.*, 1968] a major goal of collisionless shock research has been to understand the origin of the wave turbulence and its effect on the plasma. A recent study by *Scudder et al.* [1986] indicates that the primary modifications to the electron distribution function through the shock are produced by the DC magnetic and electric forces, rather than by the electrostatic waves. These forces drive the plasma to a state unstable to the growth of electrostatic waves which further modify the distribution function in a secondary yet measurable way. The electrostatic waves therefore give information regarding both the forces in the shock which drive the plasma to its unstable state and the resulting wave-induced dissipation.

A number of studies have been done regarding the electrostatic wave turbulence in the bow shock and magnetosheath. The first detailed study of the electric field spectra at the Earth's bow shock was reported by *Fredricks et al.* [1970] using OGO 5 data. From the wave spectra, it was suggested that the ion acoustic or Buneman mode was the observed wave mode. In an early study by *Rodriguez and Gurnett* [1975] using IMP 8 data it was determined that the electric field turbulence in the shock above 200 Hz was almost entirely electrostatic and polarized preferentially parallel to the static magnetic field direction. Spectra with similar shape but lower intensities were seen throughout the magnetosheath.

In a subsequent study, *Rodriguez and Gurnett* [1976] investigated possible correlations between the root-mean-square (rms) field strengths of the bow shock turbulence and solar wind parameters. Electric field strengths integrated from 20 Hz to 200 Hz and from 200 Hz to 4 kHz were used in the correlation study. One result pertaining to the electrostatic wave component (200 Hz to 4 kHz) was that the integrated rms electric field strength had a positive correlation ($r \approx 0.6$) with the electron to proton temperature ratio. This correlation is consistent with the electrostatic turbulence being ion acoustic waves, generated by an electron-proton streaming instability.

A statistical study of electrostatic turbulence in the magnetosheath was conducted by *Rodriguez* [1979]. Long-time-averaged spectra (5.46 min) were found to be combinations of three characteristic spectra: a high-frequency component ($f \geq 30$ kHz) that peaked near the plasma frequency ($f_{pe} \approx 30 - 60$ kHz), a low-frequency component that peaked below the ion plasma frequency, and an intermediate component ($f_{pi} \leq f \leq f_{pe}$). The low-frequency component was seen to resemble the shock spectra studied by *Rodriguez and Gurnett* [1975]. The high- and intermediate-frequency components were unlike spectra typically seen in the shock, but did resemble the electrostatic wave spectra seen in the foreshock region. These electrostatic waves were detected throughout the magnetosheath, well downstream from the main shock ramp free energy sources.

Rodriguez [1979] suggested that the similarities between the intermediate-frequency component and the upstream plasma waves may be an indication that a similar mechanism, i.e., beam-plasma interactions, may be generating these waves. The electric field polarization for all three components was parallel to the static magnetic field direction. It was concluded that electron plasma oscillations and ion acoustic waves were probably the wave modes found in the magnetosheath.

The discovery of electron beams parallel to the magnetic field at the Earth's bow shock [*Feldman et al.*, 1982, 1983], along with the prior observations that bow shock electrostatic waves are polarized predominantly parallel to the magnetic field, has motivated investigations of the electron beam instability. *Thomsen et al.* [1983] used model beam and background distribution functions based on the particle measurements to study the possible instabilities in the shock. Two electrostatic instabilities driven by parallel electron beams were identified: the ion acous-

[1]Space Science Division Geophysics Program, University of Washington, Seattle.
[2]Now at Los Alamos National Laboratory, Los Alamos, New Mexico.
[3]Aerospace Corporation, Los Angeles, California.
[4]Max-Planck-Institut for Extra-Terrestrial Physics, Garching, Federal Republic of Germany.
[5]Department of Physics and Astronomy, University of Iowa, Iowa City.
[6]Institute for Geophysics and Meteorology, Technical University of Braunschweig, Braunschweig, Federal Republic of Germany.
[7]Space Sciences Laboratory, University of California, Berkeley.

Paper number 89JA00505.
0148-0227/89/89JA-00505$05.00

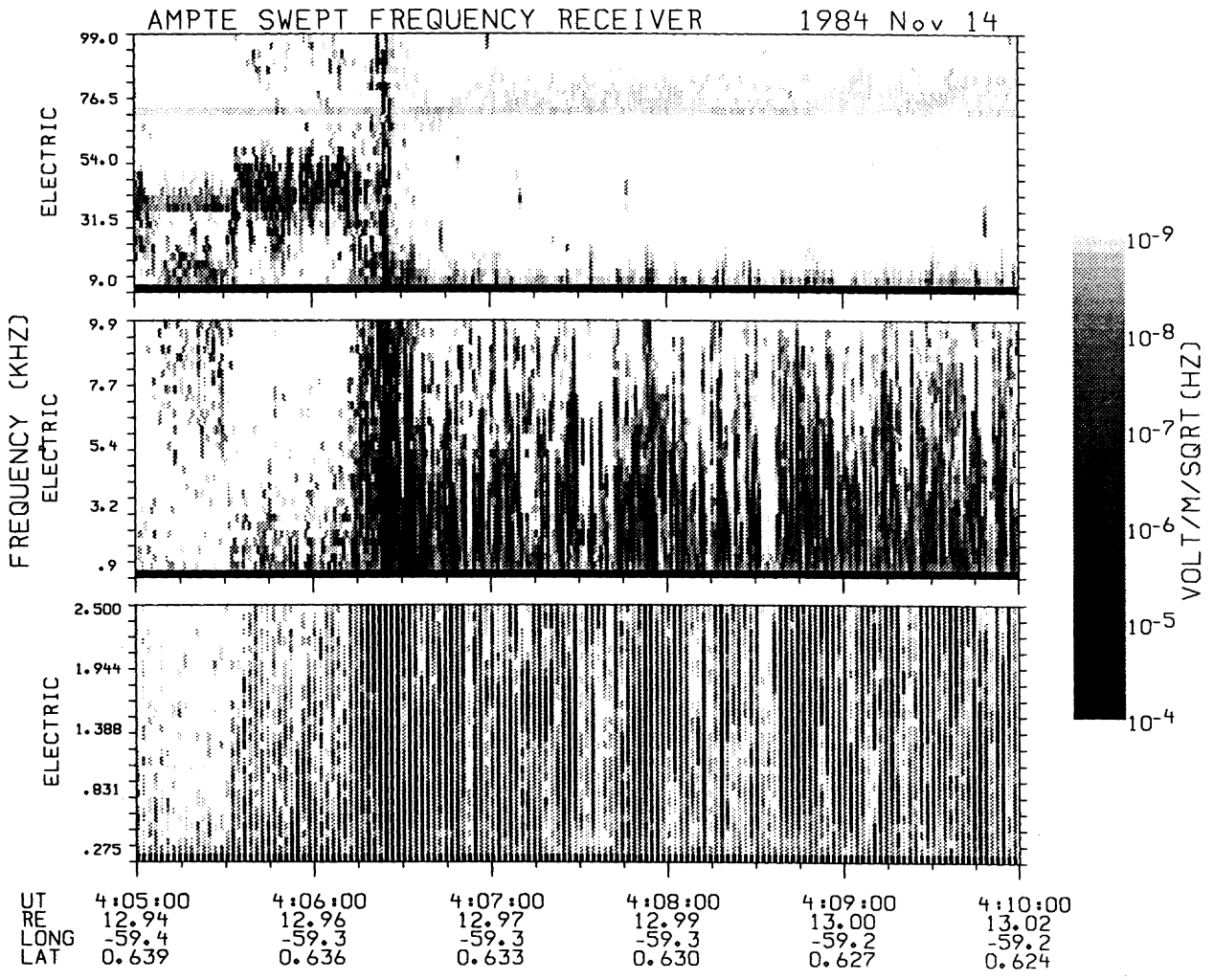

Fig. 1. Five-minute electric field spectrogram during a transition from solar wind to magnetosheath on November 14, 1984. The frequency scales are linear: 275 Hz to 2.5 kHz (lower panel), 0.9-9.9 kHz (middle panel), and 9.0-99. kHz (upper panel). Upstream (before 0406:20 UT), Langmuir oscillations are detected near approximately 36 kHz. Downstream from the shock (after 0406:30 UT), broadband bursty waves are detected up to approximately 10 kHz. Langmuir waves are detected near approximately 78 kHz.

tic and electron acoustic instabilities. These wave modes were found to be unstable up to about 3 kHz. The wave observations during the time periods considered showed that the most intense electrostatic waves had frequencies at and below about 3 kHz; however, waves were detected up to 31 kHz.

Studies of electrostatic instabilities in the presence of an electron beam have shown that the beam mode waves can have frequencies from near the ion plasma frequency to above the electron plasma frequency [*Marsh*, 1985; *Gary*, 1985]. This mode has maximum growth at phase velocities slightly below the beam velocity, and at high phase velocities it merges with the Langmuir mode.

In this study we present high frequency resolution electric field data from the Earth's bow shock and magnetosheath. These data were obtained from the stepped frequency receivers (SFRs) on board the Active Magnetospheric Particle Tracer Explorer (AMPTE) Ion Release Module (IRM) [*Häusler et al.*, 1985]. Consistent with prior research, the shock and magnetosheath electrostatic waves are seen to be very broadband, and the wave polarization is predominately parallel to the background magnetic field. We show that there is often a wide range of excited frequencies above the maximum Doppler-shifted ion acoustic frequency yet below the plasma frequency. Waves in this frequency range cannot be accounted for by either the ion acoustic or the Langmuir mode.

From the observed frequency spectra and wave polarization (parallel to the background magnetic field) we tentatively identify these high-frequency waves as the electron beam mode. The presence of waves at these frequencies is a possible indication that electron beams are present, even though the beams may not be seen in the particle measurements. This point is discussed further in the following sections. Since the electron beam mode can range from near the ion plasma frequency to above the electron plasma frequency, it is possible that much of the lower-frequency waves in the allowed range for Doppler-shifted ion acoustic waves are also the electron beam mode.

The results of a correlation study between the high-frequency electrostatic waves and various upstream solar wind and downstream magnetosheath parameters are then presented. The strongest relationships found are anticorrelations between the electrostatic wave properties and Alfven Mach number (M_A) and electron beta (β_e). The parameters M_A and β_e are very well correlated in the solar wind; therefore any correlation with M_A should also hold with β_e. It is shown that at the lower-β_e ($\beta_e \lesssim 1$) or lower-M_A ($M_A \lesssim 6$) shocks, electrostatic waves are present between the maximum frequency for Doppler-shifted ion

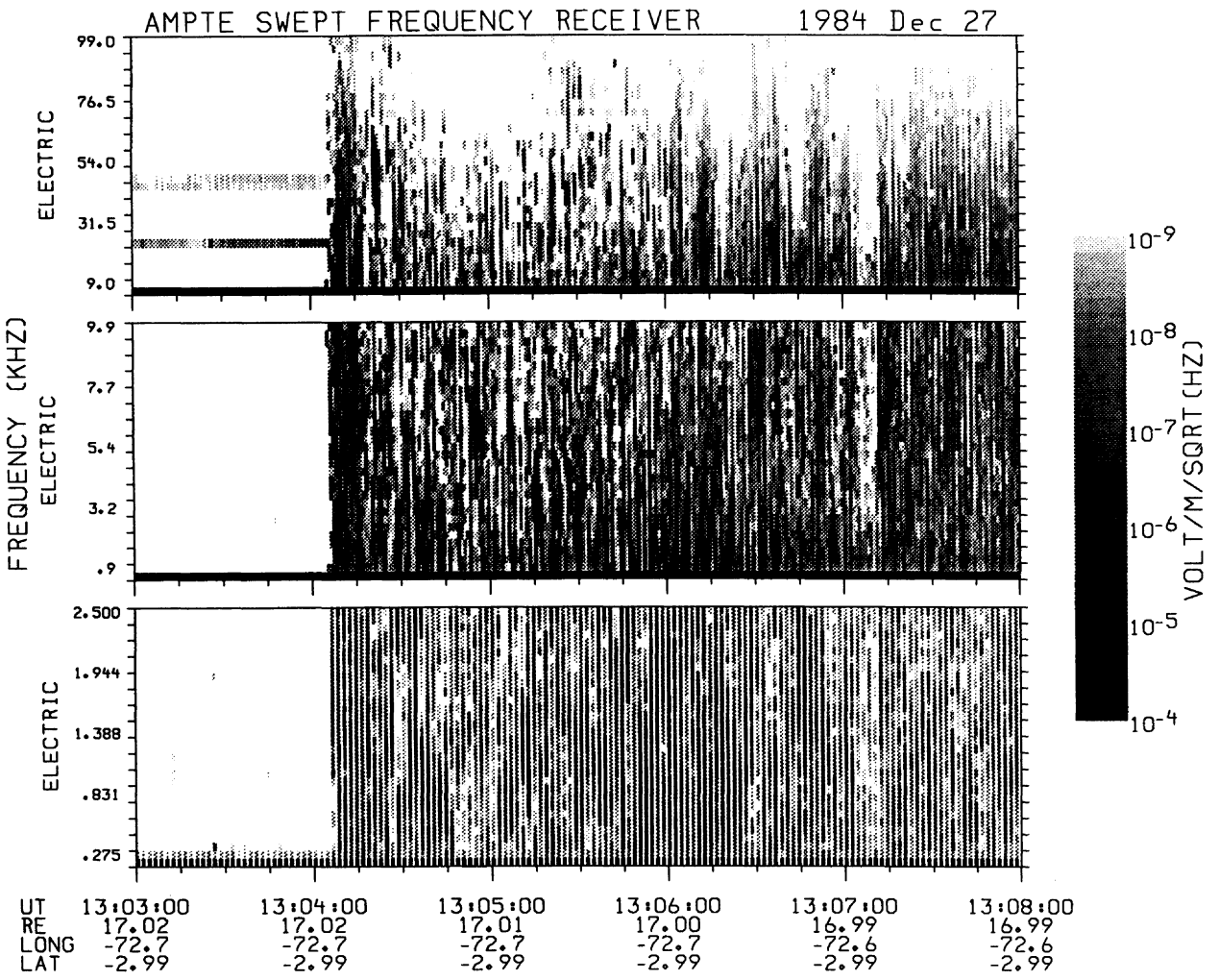

Fig. 2. Five-minute electric field spectrogram during a transition from solar wind to magnetosheath on December 27, 1984. The format is the same as in Figure 1. Upstream (before 1304:05 UT), Langmuir oscillations and oscillations at twice the plasma frequency are detected at approximately 24 kHz and 45-48 kHz. Downstream from the shock (after 1304:10 UT), broadband bursty waves are detected up to between approximately 40 kHz and 80 kHz.

acoustic waves and the plasma frequency with amplitudes as much as an order of magnitude or more above the instrument threshold. At the highest-β_e and highest-M_A shocks, electrostatic waves in this frequency range typically have very low amplitudes or are not detected at all. The results of this study are then discussed in terms of the possible wave generation mechanisms and the implications regarding the processes occurring at the shock. Three beam generation mechanisms are discussed: acceleration by the cross-shock electric field, acceleration by lower hybrid frequency waves, and a magnetosheath "time of flight" mechanism.

2. Survey of Waves Observed at the Earth's Bow Shock

In this section electric field measurements from the Earth's bow shock and magnetosheath are presented. The observed wave frequencies are compared with the plasma normal mode frequencies obtained from the measured parameters. It is demonstrated that electrostatic waves are present at frequencies above the maximum frequency for Doppler-shifted ion acoustic waves yet below the plasma frequency. Whereas previous researchers have identified the bow shock and magnetosheath electrostatic waves as either ion acoustic or Langmuir waves [*Rodriguez and Gurnett*, 1975, 1976; *Gallagher*, 1985], the analysis presented here shows that these wave modes alone cannot account for the entire measured spectra. From the measured wave spectra and polarization, the electrostatic waves with frequencies above the maximum frequency for Doppler-shifted ion acoustic waves and below the plasma frequency are tentatively identified as electron beam mode waves.

The center frequencies of the three SFRs range from 275 Hz to 99 kHz. The low-frequency SFR measures the frequency range of 275 Hz to 2525 Hz in 32 evenly spaced frequency steps every 2 s. The medium- and high-frequency SFRs measure the frequency ranges 0.9 kHz to 9.9 kHz and 9.0 kHz to 99 kHz, with each SFR sampling 32 evenly spaced frequency steps each second. The channel bandwidths for the low-, medium-, and high-frequency instruments are 100 Hz, 300 Hz, and 3 kHz, respectively. The electric field antenna is a single dipole, 47 m tip to tip. This instrument has been described by *Häusler et al.* [1985]. The vector magnetic field is obtained from three orthogonal flux gate sensors [*Lühr et al.*, 1985]. Moments of the electron and ion distribution functions are obtained from the three-dimensional plasma instrument [*Paschmann et al.*, 1985].

Five-minute electric field spectrograms from two bow shock crossings are shown in Figures 1 and 2. These spectrograms show

the full 1-s resolution of the two higher-frequency SFRs and the full 2-s resolution of the lower-frequency SFR. Both are high Alfven Mach number, quasi-perpendicular shocks. The November 14, 1984, shock (Figure 1) had $M_A \approx 15$, $\theta_{Bn} \approx 79°$, where θ_{Bn} is the angle between the average upstream magnetic field and a model shock normal [*Fairfield*, 1971], and upstream $\beta_e \approx 3.4$. The December 27, 1984, shock (Figure 2) had $M_A \approx 7$, $\theta_{Bn} \approx 86°$, and upstream $\beta_e \approx 0.7$.

A list of approximate plasma parameters on November 14, 1984, and December 27, 1984, is given in Table 1. These parameters varied considerably, particularly in the downstream region through the shock overshoot-undershoot, and are listed here only to give an indication of the approximate average values. The electron density obtained from the plasma instrument moment calculation may be below the true value because of electrons with energies below the minimum analyzer energy (15 eV). The upstream density is therefore obtained from the plasma frequency measured by the SFRs. The downstream density is obtained from the downstream plasma frequency whenever possible. However, when Langmuir waves are not clearly discernible, the downstream density is determined from the plasma instrument density with a correction based on the upstream plasma instrument density and the upstream plasma frequency, assuming that the ratio of downstream to upstream densities as measured by the plasma instrument is approximately correct.

Upstream from the November 14, 1984, shock crossing (Figure 1) Langmuir waves were detected in the solar wind (before 0406:20 UT) at approximately 39 kHz. At the shock (approximately 0406:25 UT) electric field excitations are seen throughout the entire range of the receivers (275 Hz to 99 kHz). Downstream from the shock (after 0406:30 UT) the broadband excitations are seen to be highly variable and mostly below about 10 kHz with peak amplitudes near about 1 to 3 kHz. Waves are seen at approximately 78 kHz which are interpreted to be Langmuir oscillations. The constant signal in the 72-kHz channel is due to satellite subsystem interference.

The shock crossing on December 27, 1984 (Figure 2), shows a similar wave signature; however, downstream from the shock, electric field excitations were detected at much higher frequencies than in the previous example. Upstream from the shock (before 1304:05 UT) Langmuir waves and emissions at twice the plasma frequency were detected at approximately 24 kHz and 45-48 kHz. At the shock (approximately 1304:05 UT), as in the previous example, excitations were detected throughout the range of the receivers. Downstream from the shock, waves are seen up to between about 40 kHz and 80 kHz. The downstream Langmuir waves are not always detectable in the wave data; however, based on the density measurements the plasma frequency varied between about 40 kHz and 55 kHz.

TABLE 1. Approximate Upstream and Downstream Parameters

	Nov. 14	Dec. 27
Upstream density	19 cm^{-3}	7 cm^{-3}
Downstream density	75 cm^{-3}	25 cm^{-3}
Upstream electron temperature	16 eV	23 eV
Downstream electron temperature	32 eV	75 eV
Upstream magnetic field	6 nT	10 nT
Downstream magnetic field	20 nT	38 nT
Upstream flow velocity	440 km/s	560 km/s
Downstream flow velocity	270 km/s	330 km/s
Alfven Mach number	14	7
Downstream Debye length	5 m	14 m
Maximum Doppler shift	9 kHz	4 kHz

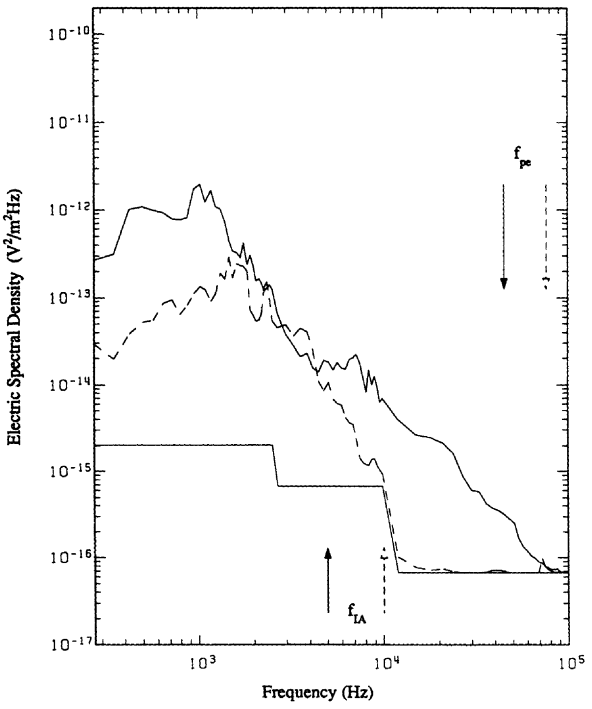

Fig. 3. One-minute averaged electric spectral density downstream from the two shock crossings shown in Figures 1 and 2: November 14, 1984, 0407-0408 (dashed curve) and December 27, 1984, 1306-1307 UT (solid curve). Indicated are approximate plasma frequencies and maximum Doppler-shifted ion acoustic frequencies. The lower line indicates the minimum detectable signal by the three SFRs.

One-minute averages of the spectral density downstream from these two shock crossings are shown in Figure 3. The dashed curve is for November 14 0407-0408 UT, and the solid curve is for December 27 1306-1307 UT. The approximate plasma frequencies, f_{pe}, and the maximum frequencies for Doppler-shifted ion acoustic waves, f_{IA}, are indicated with the dashed and solid vertical lines above and below the curves, where these lines refer to the dashed and solid curves, respectively.

The Doppler shift formula,

$$f_{sp} = f_{rest} + \frac{\mathbf{k} \cdot \mathbf{v}_{ms}}{2\pi} \tag{1}$$

gives the frequency in the spacecraft frame, f_{sp}, in terms of the plasma rest frame frequency f_{rest}, the wave number $\mathbf{k}$, and the velocity of the magnetosheath plasma $\mathbf{v}_{ms}$. The maximum frequency for Doppler-shifted ion acoustic waves is estimated from the maximum rest frame frequency, which is the ion plasma frequency f_{pi}, and the maximum Doppler shift. The maximum Doppler shift is estimated by assuming the maximum wave number to be k_D, the Debye wave number, and the wave vector direction to be along the magnetosheath plasma flow direction, $\mathbf{k} \parallel \mathbf{v}_{ms}$. The estimated maximum ion acoustic wave frequency in the spacecraft frame is then

$$f_{IA} = f_{pi} + \frac{k_D v_{ms}}{2\pi} \tag{2}$$

The Doppler shift would in most cases be much less than the estimate given here because the magnetic field is rarely aligned with the plasma flow. Nevertheless, this more conservative estimate has been used to account for the presence of waves propagating obliquely to the magnetic field, possibly along the flow direction. Although ion acoustic waves have been detected with wave vectors oblique to the magnetic field [*Gallagher*, 1985], on the average the largest amplitudes have been found to occur with the wave vectors aligned along the magnetic field [*Rodriguez*, 1979].

The electrostatic wave intensity downstream from the November 14 shock (dashed curve) had a broad peak at about 2 kHz and then decreased with increasing frequency. The upper cutoff frequency was very close to the maximum frequency for Doppler-shifted ion acoustic waves. The electrostatic wave spectrum obtained downstream from the December 27 (solid curve) shock crossing indicates that waves were present with spectral densities more than an order of magnitude above the instrument noise level in the frequency range above the maximum ion acoustic frequency ($f_{IA} \approx 5$ kHz) and below the plasma frequency ($f_{pe} \approx 45$ kHz).

Figures 1 through 3 illustrate typical electric field spectra measured by the AMPTE IRM stepped frequency receivers. Although the downstream wave spectra can at times appear to be ion acoustic waves which were Doppler-shifted by the plasma flow (as in Figure 1 and the dashed curve of Figure 3), there are many times when the waves are detected at frequencies much higher than the maximum frequency for Doppler-shifted ion acoustic waves (as in Figure 2 and the solid curve of Figure 3).

The electric field polarization for the high-frequency electrostatic waves ($f \geq 9$ kHz) detected downstream from the bow shock on December 27 is shown in Figure 4. The polarization was determined from 3 min of data, 1306-1309 UT. The electric field amplitude was obtained once every second for each of the individual frequency channels. The spin period of the spacecraft was approximately 4.4 s. A technique similar to that used by *Rodriguez* [1979] has been used to determine the polarization of the wave electric fields. By taking the data to be points in a polar coordinate system with radial distance from the origin corresponding to electric field amplitude and angle corresponding to the antenna direction at the time of the measurement (relative to a fixed reference frame), the polarization axis for the distribution of electric field amplitudes can be calculated. The polarization axis is the line in the antenna spin plane obtained by a least squares fit constrained to pass through the origin. Its uncertainty is estimated from the average distance of the measurements from the least squares fit and the sensitivity of the fit to changes in the measurements.

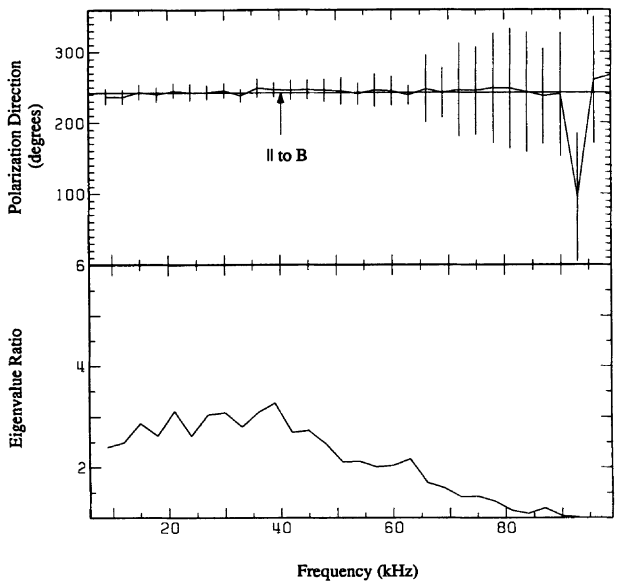

Fig. 4. Electric field polarization axis (upper panel) and eigenvalue ratio (lower panel) as functions of frequency (9.0 to 99 kHz) determined from 3 min of data on December 27, 1984, 1306-1309 UT. The polarization axis is with respect to the Earth-Sun line. The direction of the projection of the magnetic field on the antenna spin plane is indicated. The eigenvalue ratio gives an indication of the degree of polarization, with a ratio of 1 indicating an isotropic distribution of electric field amplitudes as the spacecraft rotates.

The polarization axis, the axis aligned along the dominant electric field direction, is shown as a function of frequency over 9 to 99 kHz in the upper panel of Figure 4. The direction of the magnetic field projected onto the antenna spin plane is also indicated. The eigenvalues associated with the polarization axis and the axis perpendicular to it are also obtained. The ratio of the eigenvalues gives an indication of the degree of polarization. An isotropic distribution would have a ratio of 1. The ratio of the eigenvalues is shown in the lower panel of Figure 4. The electric field is seen to be polarized predominantly parallel to the magnetic field throughout a wide range of frequencies up to about 50 kHz. The eigenvalue ratio approaches unity at the higher frequencies, indicating isotropic electric field amplitudes. For a more complete description of the polarization studies conducted in the course of this research, see *Onsager* [1988].

3. Correlations With Near-Shock Parameters

As seen in section 2, the wave spectra at and downstream from the Earth's bow shock can vary considerably from shock to shock. The goal of this section is to identify correlations between the electrostatic wave spectra and the upstream or downstream plasma parameters. This can then provide information regarding the processes occurring at and downstream from the shock which may drive the plasma to its unstable state.

This study used 45 bow shock crossings from 1984 and 1985, all with the spacecraft near the ecliptic plane ($|\lambda| < 12°$, where λ is the spacecraft latitude with respect to the ecliptic plane) and longitude ranging from 70° to −100° (GSE). The location of the shock crossings and a model bow shock [*Fairfield*, 1971] are shown in Figure 5. All of the shocks have a high Alfven Mach number ($M_A > 3$), and approximately 25% are quasi-parallel ($\theta_{Bn} \lesssim 45°$).

In order to make a quantitative comparison of the electric field spectra at different shock crossings, three characteristics of the spectra have been used. These are (1) f_{max}/f_{pe}, the approximate upper cutoff frequency of the broadband spectra normalized to the local electron plasma frequency; (2) $\varepsilon_{15\text{–}27}/n_eT_e$, the integrated electric field energy density in the frequency range 15-27 kHz normalized to the electron thermal energy density; and (3) $\varepsilon_{0.2\text{–}4}/n_eT_e$, the integrated electric field energy density in the range 275 Hz to 4 kHz normalized to the electron thermal energy density.

The frequency f_{max} is chosen to be the frequency at which the spectral density drops below 10^{-15} V^2 m^{-2} Hz^{-1}. This value is used because it is well above the instrument noise level yet near the intensities of the highest frequencies in the broadband spectra. The value of f_{max} relative to the maximum frequency for Doppler-shifted ion acoustic waves and the plasma frequency gives an indication of the presence of electrostatic waves which

are neither ion acoustic nor Langmuir waves. It should be noted that an upper cutoff frequency near the plasma frequency is not simply an indication that Langmuir waves are present. All shock crossings showing upper cutoff frequencies near or above the plasma frequency have been checked to be certain that the wave spectra are in fact broadband, extending well below the plasma frequency as well.

The 15- to 27-kHz range was chosen because for nearly all the shocks used in this study, the maximum frequency for Doppler-shifted ion acoustic waves was below this range, and the plasma frequency was above this range. It is therefore presumed that electrostatic waves in this frequency range are neither ion acoustic nor Langmuir waves. The 275-Hz to 4-kHz range was chosen to study the waves which are believed to be ion acoustic and to compare them with the results of *Rodriguez and Gurnett* [1976].

The plasma parameters used in this study are M_A, the Alfven Mach number in the spacecraft frame; M_{An}, the Alfven Mach number in the normal incidence frame; $\beta_{1e} = 8\pi n_1 T_{1e}/B_1^2$, the upstream electron beta, and β_{2e}, the downstream electron beta, where 1 and 2 refer to upstream and downstream, respectively; θ_{Bn}, the angle between the upstream magnetic field and the shock normal with the approximate shock normal determined from a model bow shock; θ_{vn}, the angle between the upstream solar wind flow velocity and the shock normal; $2\pi\lambda_D/L_a$, 2π times the downstream electron Debye length normalized to the effective antenna length where $\lambda_D = (4\pi n_{2e}e^2/T_{2e})^{1/2}$ and $L_a \approx 24$m; $(T_{2e}-T_{1e})/T_{2e}$, the electron temperature change across the shock normalized to the downstream electron temperature; T_{2e}/T_{2p}, the downstream electron to proton temperature ratio; and v_{sw}, the solar wind bulk flow speed. The plasma instrument on board the AMPTE IRM was not able to determine the proton temperature in the solar wind. Therefore, it has not been possible to determine the upstream sound speed or the fast magnetosonic Mach number.

The maximum, minimum, and average values for the plasma parameters from the 45 shock crossings are shown in Table 2. The values used in this correlation study are average values obtained by eye from 1-min intervals upstream and downstream which approximate the conditions for the shock encounter. In all cases it has been attempted to use time periods which are as close to the shock as possible yet far enough upstream and downstream that the plasma and field values are relatively steady. Because of periods when the proton instrument was not operating and times when the SFRs were in an operating mode such that the 2.5- to 4-kHz range was not measured, some of the correlation coefficients have been obtained from fewer than 45 data values. In these cases, the number of values used in the linear fit are indicated.

TABLE 2. Data Set Plasma Parameters

	Minimum	Maximum	Average
M_A	3.2	30.3	11.0
M_{An}	3.1	26.3	9.9
β_{1e}	0.29	16.8	3.0
β_{2e}	0.18	8.3	1.8
θ_{Bn}	14°	86°	56°
θ_{vn}	140°	176°	160°
$2\pi\lambda_D/L_a$	0.35	3.9	1.4
$(T_{2e}-T_{1e})/T_{2e}$	0.25	0.80	0.55
T_{2e}/T_{2p}	0.09	0.37	0.21
v_{sw} (km/s)	340	675	467

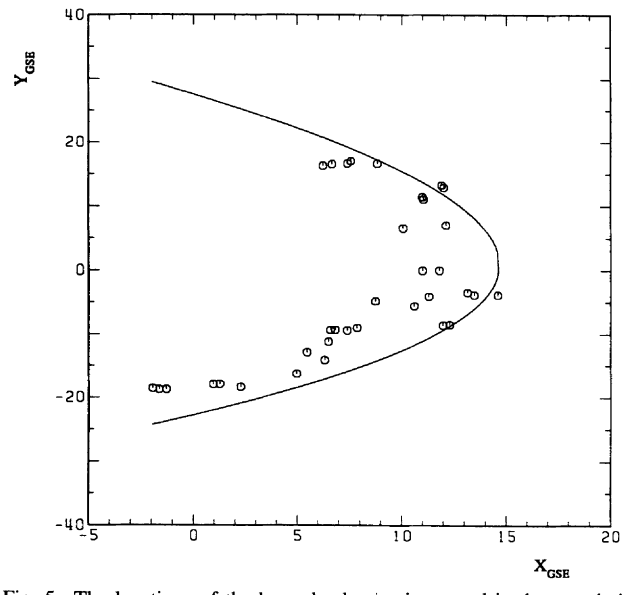

Fig. 5. The locations of the bow shock crossings used in the correlation study. These locations are the projections of the spacecraft positions onto the ecliptic plane. The solid line is the model shock determined by *Fairfield* [1971].

For each of the three electrostatic wave spectral characteristics and the plasma parameters, the correlation coefficient for the best fit straight line is obtained. The equations for the three electrostatic wave parameters are $f_{max}/f_{pe} = mx + b$, $\log_{10}(\varepsilon_{0.2-4}/n_{2e}T_{2e}) = mx + b$, and $\log_{10}(\varepsilon_{15-27}/n_{2e}T_{2e}) = mx + b$. These equations were used only to give an indication of any existing statistical relationship between the wave and plasma parameters, not because of any expected theoretical relationship.

The correlation coefficients for the linear fits are given in Table 3. The correlation coefficients which would be obtained with 1% probability from random data are 0.38 for a sample of 45 values, 0.44 for 33 values, 0.50 for 25 values, and 0.61 for 16 values [*Bendat and Piersol*, 1986]. Correlation coefficients greater than these values would be obtained with less than 1% probability from random data and are therefore considered statistically significant.

The three wave parameters are seen to be best correlated with M_A, M_{An}, β_{1e}, and β_{2e}. The correlation coefficients are negative, indicating that the highest-frequency electrostatic waves (near and above the plasma frequency) are present at and downstream from low-M_A and low-β_e shocks, and they are not present at high-M_A and high-β_e shocks. The ratio f_{max}/f_{pe} is also well correlated with $\log_{10}(\varepsilon_{15-27}/n_{2e}T_{2e})$ ($r \approx +0.93$, not shown in the table). This correlation is expected, since the averaged wave spectra typically have increasing spectral density with decreasing frequency. Therefore as f_{max} increases, the wave amplitude at any fixed frequency near and below f_{max} typically increases. The ratio f_{max}/f_{pe} is not as well correlated with $\log_{10}(\varepsilon_{0.2-4}/n_{2e}T_{2e})$ ($r \approx +0.47$).

The correlation coefficients obtained from the energy density from 275 Hz to 4 kHz are very similar to those obtained from f_{max}/f_{pe} and $\varepsilon_{15-27}/n_eT_e$. No apparent correlation is seen with T_{2e}/T_{2p}, contrary to what might be expected based on the relatively good correlation ($r \approx 0.6$) found by *Rodriguez and Gurnett* [1976] and the general belief that waves in this frequency range are ion acoustic.

TABLE 3. Correlation Coefficients

	M_A	M_{An}	β_{1e}	β_{2e}	θ_{Bn}	θ_{vn}	$\frac{2\pi\lambda_D}{L_a}$	$\frac{(T_{2e}-T_{1e})}{T_{2e}}$	T_{2e}/T_{2p}	v_{sw}
f_{max}/f_{pe}	-0.62^a	-0.66^a	-0.50	-0.60	-0.11	$+0.16^a$	+0.25	-0.11	-0.22^a	$+0.40^a$
$\log_{10}(\frac{\varepsilon_{15-27}}{n_2T_{2e}})$	-0.63^a	-0.67^a	-0.56	-0.67	-0.04	$+0.19^a$	+0.33	-0.14	-0.29^a	$+0.45^a$
$\log_{10}(\frac{\varepsilon_{0.2-4}}{n_2T_{2e}})$	-0.65^b	-0.68^b	-0.69^c	-0.73^c	$+0.09^c$	$+0.01^b$	$+0.49^c$	-0.05^c	-0.25^b	$+0.47^b$

[a] The number of data points is 33.
[b] The number of data points is 16.
[c] The number of data points is 25.

Two differences between this study and that of *Rodriguez and Gurnett* [1976] are that we have used downstream values for T_e/T_p, while they used upstream values, and we have used electrostatic wave values just downstream from the main shock ramp, while they used the peak values in the shock ramp. The ion acoustic waves in their study may have been driven by the cross-field current in the shock ramp. However, since ion acoustic waves are expected to damp very rapidly in the magnetosheath plasma, because T_e is typically of the order of T_p, the ion acoustic waves in this study are likely to have been driven by a different process.

Plots of the electrostatic wave properties versus M_A and β_{2e} are shown in Figures 6 and 7. The quasi-perpendicular shocks are indicated with circles, and the quasi-parallel shocks are indicated with plus signs. The errors bars represent the approximate variations in these values during the 1-min intervals used. Electrostatic waves tend to be present at the highest frequencies and with the highest amplitudes at the low-M_A and low-β_e shocks while waves are not present at the highest frequencies and have the lowest amplitudes at all frequencies at the high-M_A and high-β_e shocks.

To remove the strong influence of the few very high-M_A and high-β_e shocks on the correlation coefficients, we have done a similar linear fit using only the shocks with $M_A < 15$ and $\beta_e < 4$. The results using this reduced data set are shown in Table 4. The correlation coefficients for f_{max}/f_{pe} and ε_{15-27} are similar to those using the entire data set, while the correlation coefficients for $\varepsilon_{0.2-4}$ are significantly reduced. The high-frequency electrostatic

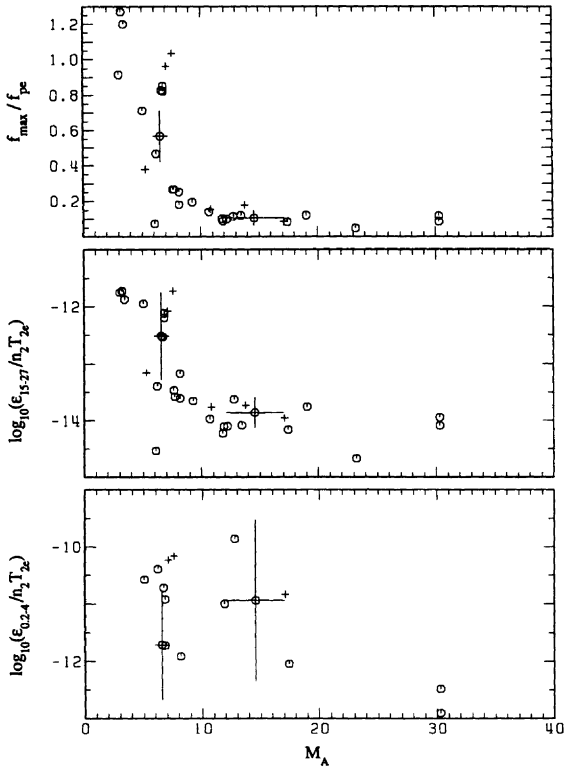

Fig. 6. Electrostatic wave upper cutoff frequency normalized to the electron plasma frequency (top panel) and integrated electric field energy density from 15 to 27 kHz (middle panel) and from 0.2 to 4 kHz (lower panel) normalized to the local electron thermal energy density versus Alfven Mach number. Quasi-perpendicular shocks are indicated with circles, and quasi-parallel shocks are indicated with plus signs.

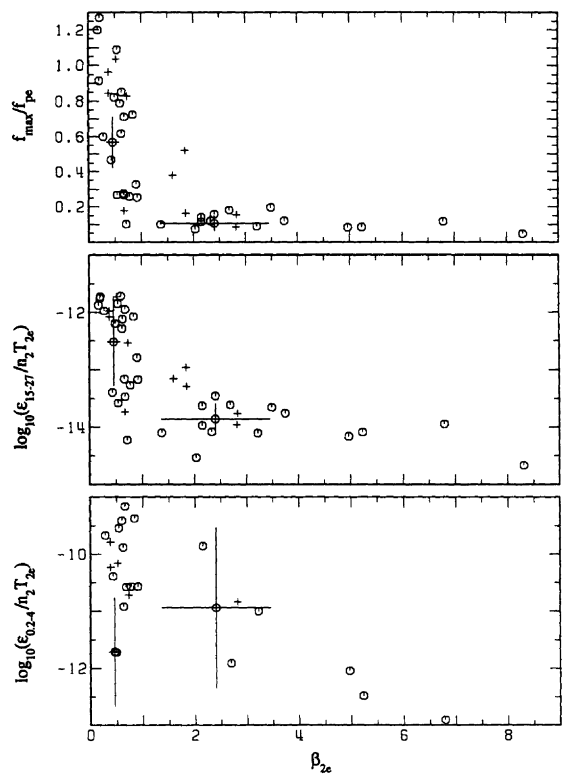

Fig. 7. Electrostatic wave upper cutoff frequency normalized to the electron plasma frequency (top panel) and integrated electric field energy density from 15 to 27 kHz (middle panel) and from 0.2 to 4 kHz (lower panel) normalized to the local electron thermal energy density versus downstream electron beta. Quasi-perpendicular shocks are indicated with circles, and quasi-parallel shocks are indicated with plus signs.

TABLE 4. Reduced Data Set Correlation Coefficients

	M_A<15	M_{An}<15	β_{1e}<4	β_{2e}<4
f_{max}/f_{pe}	−0.75[a]	−0.78[b]	−0.63[c]	−0.69[d]
$\log_{10}(\varepsilon_{15-27}/n_2T_{2e})$	−0.73[a]	−0.75[b]	−0.63[c]	−0.69[d]
$\log_{10}(\varepsilon_{0.2-4}/n_2T_{2e})$	+0.14[e]	−0.22[f]	−0.18[g]	−0.38[h]

[a] The number of data points is 27.
[b] The number of data points is 29.
[c] The number of data points is 37.
[d] The number of data points is 41.
[e] The number of data points is 12.
[f] The number of data points is 14.
[g] The number of data points is 20.
[h] The number of data points is 22.

wave amplitudes and upper cutoff frequencies appear correlated with M_A and β_e over the full range of values for these parameters. The good correlation found between the low-frequency wave intensities and M_A and β_e appears to be due to the few shocks with very high M_A and β_e for which the wave intensities are low at all frequencies.

4. Analysis of the Electron Beam Mode

In this section the electron beam mode is studied to investigate the possibility that the waves between the maximum frequency for Doppler-shifted ion acoustic waves and Langmuir waves could be driven by electron beams. The dependence of f_{max} on the plasma parameters is also investigated. Solutions of the one-dimensional linear Vlasov equation for a homogeneous plasma consisting of Maxwellian background electrons and ions and a Maxwellian electron beam are presented. The following analysis shows that the electron beam instability can result in broadband growth. We derive for a simple case an expression for f_{max}, the upper cutoff frequency for the growing broadband waves, as a function of the beam and background parameters.

The parameters used here to study the electron beam instability, although similar to parameters which have been reported, are not intended to represent a fit to a measured distribution function. The main point is to demonstrate that this mode of the dispersion relation can be unstable over a wide range of frequencies, particularly those frequencies inaccessible by the ion acoustic and Langmuir modes, and to note how the instability varies with the beam and background parameters.

As pointed out by *Rodriguez* [1979], the wave spectra in the magnetosheath are similar to those seen upstream in the foreshock. The foreshock electrostatic waves are thought to be generated by parallel electron beams [*Etcheto and Faucheux*, 1984; *Lacombe et al.*, 1985; *Fuselier et al.*, 1985]. As is typically the case downstream from the main shock ramp as well as downstream from the electron foreshock boundary, the electrostatic waves are present over a broad frequency range, from below the ion plasma frequency to above the electron plasma frequency, in regions where unstable features of the electron distribution function are often not detected.

Therefore, as is thought to be the case in the electron foreshock, the electrostatic waves at and downstream from the main shock ramp could result from low-density, cold features on the electron distribution function which are present over time scales that are long compared to the growth periods of the waves (10^{-3} s) yet short compared to the time required to obtain a measurement of the distribution function (about 5 s). Rather than attempt to model the electron distribution function, some general parameter dependencies of the electron beam instability will be presented and compared with the measured wave spectra.

The background electron and ion distribution functions are given by

$$f_{i,e} = (2\pi v_{ti,te}^2)^{-1/2}\exp\left[-\frac{v^2}{2v_{ti,te}^2}\right] \tag{3}$$

and the beam electrons by

$$f_b = (2\pi v_{tb}^2)^{-1/2}\exp\left[-\frac{(v-v_b)^2}{2v_{tb}^2}\right] \tag{4}$$

where $v_{t\alpha} = (T_\alpha/m_\alpha)^{1/2}$ are the species thermal velocities, with T_α in energy units, and v_b is the beam drift velocity. For these particle distributions the dielectric function can be written

$$\varepsilon(k, \omega) = 1 + \frac{k_e^2}{k^2}W(z_e) + \frac{k_i^2}{k^2}W(z_i) + \frac{k_b^2}{k^2}W(z_b) \tag{5}$$

where $k_\alpha = (4\pi n_\alpha e^2/T_\alpha)^{1/2}$ is the Debye wave number for each species, $\omega = \omega_r + i\omega_i$ is the complex frequency, $z_{i,e} = \omega/kv_{ti,te}$, $z_b = (\omega - kv_b)/kv_{tb}$, and $W(z_\alpha)$ is the plasma dispersion function [*Ichimaru*, 1973]. The dispersion relation is given by $\varepsilon(k, \omega) = 0$.

To illustrate the range of unstable wave frequencies due to the electron beam instability, a simple case is considered. For the analysis of the higher-frequency electrostatic waves ($\omega_r \approx \omega_{pe}$), the ion contribution to the dispersion relation can be neglected, giving

$$0 = 1 + \frac{k_e^2}{k^2}W(z_e) + \frac{k_b^2}{k^2}W(z_b) \tag{6}$$

To simplify further the dispersion relation, $k_e^2 = k_b^2$ will be assumed. This assumption is satisfied when

$$\frac{T_b}{T_e} = \frac{n_b}{n_e} \tag{7}$$

and would be valid, for example, in the case of a cold, tenuous beam. The dispersion relation then becomes

$$k^2 = -k_e^2[W(z_e) + W(z_b)] \tag{8}$$

The upper cutoff frequency for the broadband growing waves can be determined by finding the real frequency for which the imaginary frequency passes through zero. The dependence of the upper cutoff frequency on the various plasma parameters can be determined by solving the dispersion relation at the point where $\omega_i = 0$. When $\omega_i = 0$, the plasma dispersion function has the following properties [*Ichimaru*, 1973]:

$$\mathrm{Re}W(z) = \mathrm{Re}W(-z) \tag{9}$$

$$\mathrm{Im}W(z) = -\mathrm{Im}W(-z) \tag{10}$$

The solution to the imaginary part of the dispersion relation is $z_b = -z_e$. The real part of the dispersion relation then becomes

$$k^2 = -2k_e^2W(z_e) \tag{11}$$

Using the relation $z_e = \omega/kv_e$, this can be expressed in terms of frequency:

$$\omega_r^2/\omega_{pe}^2 = -2z_e^2 W(z_e) \tag{12}$$

The real frequency takes on its maximum value of $\omega_{max}/\omega_{pe} \approx 1.8$ at $z_e \approx 2.76$. With the solution $z_e = -z_b$ this expression can be written in terms of v_b/v_{te}, the ratio of beam velocity to background electron thermal velocity,

$$\omega_{max}^2/\omega_{pe}^2 = -2(v_b/v_{te})^2[1+(T_b/T_e)^{1/2}]^{-2}$$

$$W\{(v_b/v_{te})[1+(T_b/T_e)^{1/2}]^{-1}\} \tag{13}$$

The upper cutoff frequency as a function of v_b/v_{te} for $T_b/T_e = n_b/n_e = 0.1$ is shown in Figure 8. For low beam velocities, the upper cutoff frequency is seen to increase with increasing beam velocity. At the higher beam velocities the upper cutoff frequency decreases, approaching the plasma frequency as the beam mode merges with the Langmuir mode. Also shown in Figure 8 are curves for different temperature ratios with $n_b/n_e = 0.1$. For T_b/T_e not equal to n_b/n_e, (13) is no longer valid, and the full dispersion relation must be solved. However, the dispersion relation is still greatly simplified by the assumption that $\omega_i = 0$. As the beam to background temperature ratio decreases, the instability becomes active at lower beam velocities. Curves similar to those in Figure 8 are shown in Figure 9, for different values of n_b/n_e with $T_b/T_e = 0.1$. As n_b/n_e increases, the instability becomes active at lower beam velocities.

The results shown here demonstrate the dependence of the electron beam mode upper cutoff frequency on the beam and background plasma parameters. These results are similar to those demonstrated by *Thomsen et al.* [1983], in which the electron acoustic mode growth rate was shown to increase with increasing beam velocity and density and with decreasing beam temperature.

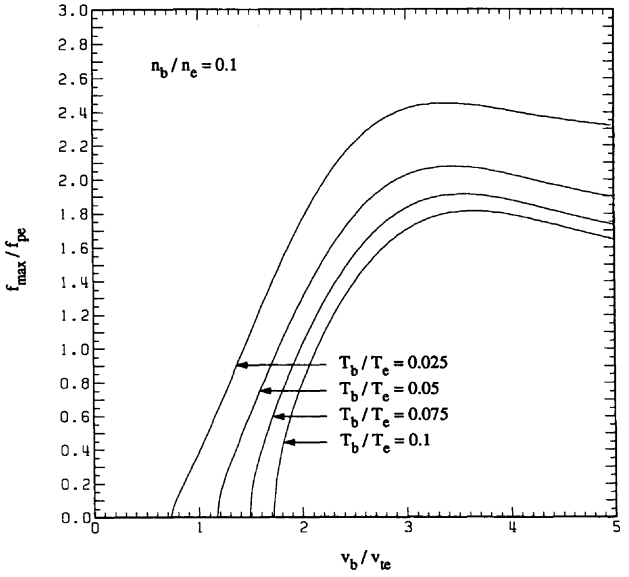

Fig. 8. Maximum unstable frequency (normalized to the electron plasma frequency) as a function of beam velocity (normalized to the background electron thermal velocity) for a density ratio of 0.1 and four temperature ratios. For a given temperature ratio, the maximum frequency increases rapidly at lower beam velocities. As the beam temperature is decreased, instability occurs at lower beam velocities.

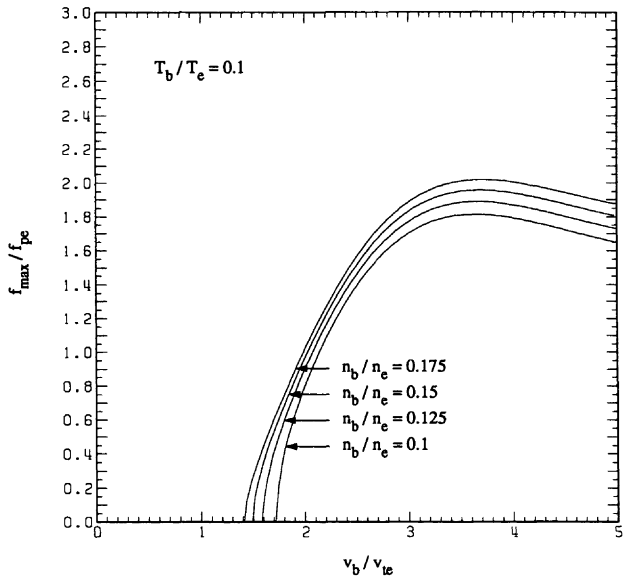

Fig. 9. Maximum unstable frequency (normalized to the electron plasma frequency) as a function of beam velocity (normalized to the background electron thermal velocity) for a temperature ratio of 0.1 and four density ratios. For a given density ratio, the maximum frequency increases rapidly at lower beam velocities. As the beam density is increased, instability occurs at lower beam velocities.

In the simple case investigated, the electron beam mode is seen to have the following properties:

1. The unstable waves can be very broadband, ranging from low frequencies to above the electron plasma frequency.

2. For low beam velocities ($v_b \lesssim 3v_{te}$), the upper cutoff frequency of the broadband growth increases with increasing beam velocity, increasing beam density, or decreasing beam temperature.

Therefore when the electron beam instability is operating, it is reasonable to expect broadband waves polarized along the beam direction (the magnetic field direction), with an upper cutoff frequency which varies with the beam parameters. Figures 8 and 9 indicate that the electron beam mode waves may be unstable in the frequency range inaccessible to the ion acoustic and Langmuir modes and that variations in the beam and background plasma parameters could account for the large variations in the wave spectra at the different shock crossings.

5. SUMMARY OF OBSERVATIONS

The Earth's bow shock and magnetosheath are typically characterized by high-amplitude broadband electrostatic waves. The excellent frequency resolution of the stepped frequency receivers on board the AMPTE IRM has allowed for an investigation of the high-frequency waves in greater detail than has previously been possible. The wave spectra presented here show some features which support previous research, as well as others which have not previously been reported.

Similar to prior results [*Rodriguez and Gurnett,* 1975, 1976; *Rodriguez,* 1979], the electrostatic waves at and downstream from the shock are shown to be broadband, impulsive in time, and polarized predominantly parallel to the background magnetic field. The waves are detected at frequencies as low as 275 Hz (the minimum SFR frequency) up to above the plasma frequency ($f_{pe} \approx 40 - 60$ kHz). We have concentrated primarily on the higher-frequency waves ($f \gtrsim 9$ kHz) and on the variations in wave intensities seen at different shock crossings.

The first point we have made is that the maximum frequency for Doppler-shifted ion acoustic waves and the plasma frequency are usually well separated. For example, on December 27, 1984 (see Figures 2 and 3), $f_{IA} = f_{pi} + k_D v_{ms} \approx 5$ kHz and $f_{pe} \approx 45$ kHz. The AMPTE IRM SFRs have a total of 27 channels between these frequencies. The electric field fluctuations in this frequency range, which is inaccessible to either the ion acoustic or Langmuir modes, are clearly resolved. The electrostatic wave measurements presented here demonstrate that the ion acoustic and Langmuir modes alone cannot account for the entire measured spectra. The wave polarization in the frequency range inaccessible to the ion acoustic and Langmuir modes is predominantly parallel to the magnetic field.

In a plasma with the plasma frequency much greater than the electron cyclotron frequency (typically $f_{pe} \approx 50 f_{ce}$) there are only two known electrostatic wave modes with frequencies ranging from far below the plasma frequency up to and above it. These are the Bernstein mode or electron cyclotron harmonics and the electron beam mode. The Bernstein mode is known to propagate predominantly perpendicular to the magnetic field [*Krall and Trivelpiece,* 1986], which is inconsistent with the present observations. The electron beam mode is polarized in the direction of the beam, which would typically be along the magnetic field. Therefore, from the observed frequency range and polarization it is concluded that the most likely wave mode present at and downstream from the shock in the frequency range inaccessible to the ion acoustic and Langmuir modes is the electron beam mode.

In the absence of an electron beam, electric field fluctuations in this inaccessible frequency range would be heavily damped [cf. *Marsch,* 1985]. Since the waves are seen to persist far downstream from the shock, (Figure 2; see also *Rodriguez,* [1979]), the convection of shock-generated waves in a stable magnetosheath plasma is not a likely explanation. Our interpretation would imply then that the presence of electrostatic waves at these frequencies indicates the presence of local unstable features in the electron distribution function, or beams.

A correlation study has also been presented, investigating the processes which could give rise to electron beams. The strongest relationship found between the electrostatic wave properties and plasma parameters was with M_A and β_e. The correlations were negative, reflecting the decrease in wave amplitudes and upper cutoff frequencies with increasing M_A and β_e. No significant relationship was seen between the wave properties and θ_{Bn}, T_{2e}/T_{2p}, λ_D, θ_{vn}, $(T_{2e}-T_{1e})/T_{2e}$, or v_{sw}.

In the following section the correlation study results are discussed in terms of various mechanisms which may produce electron beams at and downstream from the shock. Two previously proposed shock acceleration mechanisms are discussed: the cross-shock electric field and lower hybrid frequency waves, as well as a new mechanism in analogy to the foreshock time of flight mechanism [*Filbert and Kellogg,* 1979]. The proposed magnetosheath time of flight mechanism may account for the generation of electrostatic waves far downstream from the shock, even in the absence of beams being produced at the shock.

6. Discussion of Possible Beam Generation Mechanisms

Electron beams have been measured near the main shock ramp where the electrostatic wave amplitudes are usually highest [*Feldman,* 1985; *Scudder et al.,* 1986]. However, measurements downstream from the shock typically give no indication of unstable particle distributions [*Feldman,* 1985]. *Thomsen et al.* [1985] reported one case where parallel cuts of two-dimensional electron distribution functions showed downstream directed beams in the shock ramp and shock-directed beams just downstream from the shock. *Feldman* [1985] suggested that the shock-directed beams could be electrons accelerated into the magnetosheath at the other intersection of the magnetic field line with the curved shock.

One mechanism which has been proposed to explain the observed beams is the acceleration of electrons by the cross-shock electric field [*Feldman,* 1985]. Electrons in the upstream region flowing along the magnetic field toward the shock would be accelerated into the downstream region. These electrons could then appear as a beam to the hotter downstream plasma.

If the relevant acceleration mechanism were the cross-shock electric field, the observed correlations may be an indication that the cross-shock electric field in the de Hoffman-Teller frame decreases with increasing M_A or β_e. A similar effect has been seen in the normal incidence frame with computer simulations [*Leroy et al.,* 1982]. The normal incidence frame cross-shock potential normalized to the incident flow energy has been shown to decrease with increasing Alfven Mach number above $M_A \approx 6$. This is believed to result from the increased effect of the reflected ions on the incoming solar wind flow at the higher Mach numbers.

One problem with this interpretation is the lack of correlation between the high-frequency electrostatic waves and the normalized electron temperature jump across the shock. The ratio of the electron temperature change across the shock to the downstream electron temperature, $(T_{2e}-T_{1e})/T_{2e}$, is proportional the ratio of the electron energy gain in crossing the shock to the downstream particle energy. For a quasi-perpendicular shock in which the electron motion is adiabatic, the electron energy gain in crossing the shock is approximately given by the cross-shock potential energy jump in the de Hoffman-Teller frame [*de Hoffman and Teller,* 1950; *Goodrich and Scudder,* 1984]:

$$[e\phi^{HT}]_1^2 \approx \frac{\gamma}{\gamma-1}[T_e]_1^2 \tag{14}$$

where γ is the ratio of specific heats and $[\ ]_1^2$ signifies the difference between the downstream and upstream values. As the upstream parallel electrons cross the shock, they will be accelerated into the downstream region and may appear as a beam with velocity v_b, given approximately by

$$\frac{1}{2}m_e v_b^2 \approx \frac{\gamma}{\gamma-1}[T_e]_1^2 \tag{15}$$

As shown in section 4, an important parameter for the electron beam instability is the ratio of the beam velocity to background thermal velocity. Therefore if the observed electrostatic waves are generated by electrons accelerated along the magnetic field by the cross-shock electric field, we might expect to see a positive correlation with $(T_{2e}-T_{1e})/T_{2e}$. The observed correlations, however, are low and negative. Acceleration of electrons by the cross-shock electric field may still be an important mechanism for the observed electrostatic wave generation; however, the direct association between the magnitude of the cross-shock potential and the high-frequency electrostatic waves is not apparent.

It has also been shown that waves in the lower hybrid frequency range generated by the modified two-stream instability may create electron beams [*Tanaka and Papadopoulos,* 1983].

This mechanism was discussed by *LaBelle et al.* [1987] as a possible explanation for the broadband spikelike electrostatic waves seen near flux transfer events. These waves are very similar to those seen in the magnetosheath and bow shock. As pointed out by these authors, the beams would not be detectable by the plasma instrument because their time scale would be very short, similar to that of the waves, which is much shorter than the resolution of the plasma instrument.

If the electron beams were generated by lower hybrid frequency waves, the observed correlation could be an indication that this mechanism becomes ineffective at the higher-M_A or higher-β_e shocks. There is both experimental [*Mellott and Greenstadt,* 1988] and theoretical [*Winske,* 1985; *Gary et al.,* 1987] evidence that the lower hybrid frequency waves have lower amplitudes at the high-β_e shocks. *Mellott and Greenstadt* [1988] investigated the correlations between upstream solar wind parameters and lower hybrid frequency waves in the shock foot and ramp. The best correlations found between the wave electric field amplitudes in the ramp and the plasma parameters were with normal solar wind flow velocity (r = +0.81) and electron beta (r = -0.62). The theoretical analyses indicate that the linear growth rates for the lower hybrid like waves decrease with increasing β_e [*Winske,* 1985; *Gary et al.,* 1987] and increase with increasing velocity between the solar wind and the reflected ions [*Gary et al.,* 1987]. Our study indicates a positive although low correlation with solar wind velocity.

Another possibility is that the unstable distributions result from a time of flight mechanism similar to those in the Earth's foreshock [*Filbert and Kellogg,* 1979]. Since the shock may not be spatially or temporally uniform, it is likely that the shock surface has discontinuities in the plasma parameters. Spatial discontinuities in the shock could correspond to spatial discontinuities in the distribution of electrons being accelerated downstream. These spatial boundaries could then give rise to downstream particle distributions similar to those seen in the foreshock. These discontinuities could result through either the dynamics of the shock itself or from magnetic field and plasma discontinuities continually impinging on the shock from the incoming solar wind.

Locations in the magnetosheath which are magnetically connected to the upstream edge of shock regions with higher downstream directed electron fluxes would be analogous to the upstream boundary of the foreshock. Downstream from these locations the competition between the electrons' steaming velocities along the magnetic field and the convection velocity of the magnetic field could result in particle distributions that are unstable to electrostatic wave growth. Rather than one upstream boundary as at the foreshock, there could be many analogous boundaries downstream. The location of these boundaries could change very rapidly in time, resulting in very short time scale bursts of electrostatic waves, as is observed.

This mechanism would not require shock acceleration to directly produce beams. Stable suprathermal tails at the shock could result in beams farther downstream through the time of flight mechanism, provided boundaries were present separating regions with differing electron fluxes at the higher energies. A more detailed description of this mechanism will be the subject of a forthcoming publication.

In conclusion, the frequency range and polarization of the electrostatic waves presented in this paper are consistent with the interpretation that electron beam mode waves are present at and downstream from the Earth's bow shock. Linear Vlasov theory shows that the electron beam mode may be unstable in the observed frequency ranges and that variations in the beam parameters can account for the large variations seen in the wave spectra at different shock crossings. A correlation study using 45 shock crossings indicates that the electrostatic wave upper cutoff frequencies and amplitudes are anticorrelated with M_A and β_e. Various possible beam generation mechanisms have been discussed in terms of the correlation study results.

More work needs to be done before a conclusive identification of the electrostatic wave modes and generation mechanisms at and downstream from the shock can be made. In particular, detailed comparisons of the electrostatic wave spectra and particle distributions at and downstream from the shock are essential in determining if the electrostatic waves are in fact generated by electron beams. Once the wave modes are identified, the effects of the waves on the plasma can be evaluated, and the issues of beam persistence far downstream from the shock can be addressed. Although the role of electrostatic waves in the plasma heating at shocks has recently been called into question [*Scudder et al.,* 1986; *Mellott,* 1986], the wave spectra do vary considerably at collisionless shocks and therefore present valuable clues toward understanding the large- and small-scale processes occurring in the collisionless plasma.

Acknowledgments. One author (T.G.O.) would like to acknowledge numerous discussions with Michael McCarthy which contributed greatly to this research. The authors also thank the two referees for their helpful comments and suggestions. This research was supported at the University of Washington by the National Aeronautics and Space Administration under grant NAGW-1218 and the Office of Naval Research (ONR) under contract N00014-84-K-0160. The research at the University of Iowa was supported by ONR contract N00014-85-K-040 and NASA grants NGL-16-001-043 and NGL-16-001-002. The research at the Aerospace Corporation was supported in part by ONR and in part by the U.S. Systems Command under contract F04701-85-C-0086. The research at the University of California, Berkeley, was supported by NASA grant NGL-05-003-017.

The Editor thanks C. Lacombe and M. M. Mellott for their assistance in evaluating this paper.

REFERENCES

Bendat, J. S., and A. G. Piersol, *Random Data,* John Wiley, New York, 1986.

de Hoffman, F., and E. Teller, Magneto-hydromagnetic shocks, *Phys. Rev., 80,* 692, 1950.

Etcheto, J., and M. Faucheux, Detailed study of electron plasma waves upstream of the Earth's bow shock, *J. Geophys. Res., 89,* 6631, 1984.

Fairfield, D. H., Average and unusual locations of the Earth's magnetopause and bow shock, *J. Geophys. Res., 76,* 6700, 1971.

Feldman, W. C., Electron velocity distributions near collisionless shocks, in *Collisionless Shocks in the Heliosphere: Reviews of Current Research, Geophys. Monogr. Ser., vol. 35,* edited by B. T. Tsurutani and R. G. Stone, pp. 195-205, AGU, Washington, D. C., 1985.

Feldman, W. C., S. J. Bame, S. P. Gary, J. T. Gosling, D. McComas, M. F. Thomsen, G. Paschmann, N. Sckopke, M. M. Hoppe, and C. T. Russell, Electron heating within the Earth's bow shock, *Phys. Rev. Lett., 49,* 199, 1982.

Feldman, W. C., R. C. Anderson, S. J. Bame, S. P. Gary, J. T. Gosling, D. J. McComas, M. F. Thomsen, G. Paschmann, and M. M. Hoppe, Electron velocity distributions near the Earth's bow shock, *J. Geophys. Res., 88,* 96, 1983.

Filbert, P. C., and P. J. Kellogg, Electrostatic noise at the plasma frequency beyond the Earth's bow shock, *J. Geophys. Res., 84.,* 1369, 1979.

Fredricks, R. W., C. F. Kennel, F. L. Scarf, G. M. Crook, and I. M. Green, Detection of electric field turbulence in the Earth's bow shock, *Phys. Rev. Lett., 21,* 1761, 1968.

Fredricks, R. W., G. M. Crook, C. F. Kennel, I. M. Green, F. L. Scarf, P. J. Coleman, and C. T. Russell, OGO 5 observations of electrostatic turbulence in bow shock magnetic structures, *J. Geophys. Res., 75,* 3751, 1970.

Fuselier, S. A., D. A. Gurnett, and R. J. Fitzenreiter, The downshift of electron plasma oscillations in the electron foreshock region, *J. Geophys. Res., 90,* 3935, 1985.

Gallagher, D. L., Short-wavelength electrostatic waves in the Earth's magnetosheath, *J. Geophys. Res., 90,* 1435, 1985.

Gary, S. P., Electrostatic instabilities in plasmas with two electron components, *J. Geophys. Res., 90,* 8213, 1985.

Gary, S. P., R. L. Tokar, and D. Winske, Ion/ion and electron/ion cross-field instabilities near the lower hybrid frequency, *J. Geophys. Res., 92,* 10,029, 1987.

Goodrich, C. C. and J. D. Scudder, The adiabatic energy change of plasma electrons and the frame dependence of the cross-shock potential at collisionless magnetosonic shock waves, *J. Geophys. Res., 89,* 6654, 1984.

Häusler, B., R. R. Anderson, D. A. Gurnett, H. C. Koons, R. H. Holzworth, O. H. Bauer, R. Treumann, K. Gnaiger, D. Odem, W. B. Harbridge, and F. Eberl, The plasma wave instrument on board the AMPTE IRM satellite, *IEEE Trans. Geosci. Remote Sens., GE-23,* 267, 1985.

Ichimaru, S., *Basic Principles of Plasma Physics: A Statistical Approach,* W. A. Benjamin, Reading, Mass., 1973.

Krall, N. A., and A. W. Trivelpiece, *Principles of Plasma Physics,* p. 407, San Francisco Press, San Francisco, Calif., 1986

LaBelle, J., R. A. Treumann, G. Haerendel, O. H. Bauer, G. Paschmann, W. Baumjohann, H. Lühr, R. R. Anderson, H. C. Koons, and R. H. Holzworth, AMPTE IRM observations of waves associated with flux transfer events in the magnetosphere, *J. Geophys. Res., 92,* 5827, 1987.

Lacombe, C., A. Mangeney, C. C. Harvey, J. D. Scudder, Electron plasma waves upstream of the Earth's bow shock, *J. Geophys. Res., 90,* 73, 1985.

Leroy, M. M., D. Winske, C. C. Goodrich, C. S. Wu, and K. Papadopoulos, The structure of perpendicular bow shocks, *J. Geophys. Res., 87,* 5081, 1982.

Lühr, H., N. Klöcker, W. Oelschlägel, B. Häusler, and M. Acuna, The IRM fluxgate magnetometer, *IEEE Trans. Geosci. Remote Sens., GE-23,* 259, 1985.

Marsch, E., Beam-driven electron acoustic waves upstream of the Earth's bow shock, *J. Geophys. Res., 90,* 6327, 1985.

Mellott, M. M., Plasma wave signatures of collisionless shocks and the role of plasma wave turbulence in shock formation, *Adv. Space Res., 6,* 25, 1986.

Mellott, M. M., and E. W. Greenstadt, Plasma waves in the range of the lower hybrid frequency: ISEE 1 and 2 observations at the Earth's bow shock, *J. Geophys. Res., 93,* 9695, 1988.

Onsager, T. G., Plasma waves in the Earth's foreshock, bow shock, and magnetosheath, Ph.D. Dissertation, Univ. of Washington, Seattle, 1988.

Paschmann, G., H. Loidl, P. Obermayer, M. Ertl, R. Laborenz, N. Sckokpe, W. Baumjohann, C. W. Carlson and D. W. Curtis, The plasma instrument on board the AMPTE IRM satellite, *IEEE Trans. Geosci. Remote Sens.,* GE-23, 262-266, 1985.

Rodriguez, P., Magnetosheath electrostatic turbulence, *J. Geophys. Res., 84,* 917, 1979.

Rodriguez, P., and D. A. Gurnett, Electrostatic and electromagnetic turbulence associated with the Earth's bow shock, *J. Geophys. Res., 80,* 19, 1975.

Rodriguez, P., and D. A. Gurnett, Correlation of bow shock plasma wave turbulence with solar wind parameters, *J. Geophys. Res., 81,* 2871, 1976.

Scudder, J. D., A. Mangeney, C. Lacombe, C. C. Harvey, C. S. Wu, and R. R. Anderson, The resolved layer of a collisionless, high β, supercritical, quasi-perpendicular shock wave, 3, Vlasov electrodynamics, *J. Geophys. Res., 91,* 11,075, 1986.

Tanaka, M., and K. Papadopoulos, Creation of high-energy electron tails by means of the modified two-stream instability, *Phys. Fluids, 26,* 1697, 1983.

Thomsen, M. F., H. C. Barr, S. P. Gary, W. C. Feldman, and T. E. Cole, Stability of electron distributions within the Earth's bow shock, *J. Geophys. Res., 88,* 3035, 1983.

Thomsen, M. F., J. T. Gosling, S. J. Bame, and M. M. Mellott, Ion and electron heating at collisionless shocks near the critical Mach number, *J. Geophys. Res., 90,* 137, 1985.

Winske, D., Microtheory of collisionless shock current layers, in *Collisionless Shocks in the Heliosphere: Reviews of Current Research, Geophys. Monogr. Ser., vol. 35,* edited by B. T. Tsurutani and R. G. Stone, pp. 225-236, AGU, Washington, D. C., 1985.

R. R. Anderson and D. A. Gurnett, Department of Physics and Astronomy, University of Iowa, Iowa City, IA 52242.

O. H. Bauer, Max-Planck-Institut for Extra-Terrestrial Physics, Garching 8046, Federal Republic of Germany.

C. W. Carlson, Space Sciences Laboratory, University of California, Berkeley, CA 94720.

R. H. Holzworth, Space Science Division, Geophysics Program, AK-50, University of Washington, Seattle, WA 98195.

H. C. Koons, Aerospace Corporation, M2-260, P. O. Box 92957, Los Angeles, CA 90009.

H. Lühr, Institute for Geophysics and Meteorology, Technical University of Braunschweig, 3300 Braunschweig, Federal Republic of Germany.

T. G. Onsager, Los Alamos National Laboratory, ESS-8, MS-D438, Los Alamos, NM 87545.

(Received January 15, 1988;
revised February 16, 1989;
accepted March 9, 1989.)